LETTERS
PUBLISHED ONLINE: 30 MARCH 2014 | DOI: 10.1038/NGEO2120

nature geoscience

Chemical complexity of hotspots caused by cycling oceanic crust through mantle reservoirs

Mingming Li*, Allen K. McNamara and Edward J. Garnero

Lavas erupted at ocean island hotspots such as Hawaii have diverse geochemical signatures. These ocean island basalts are thought to be derived from many sources with different chemical compositions within Earth's mantle and contain components of more primitive, less degassed material, as well as several recycled oceanic crustal components[1–3]. Furthermore, the recycled oceanic crustal components display vastly different ages[4,5]. The various components may be derived from different mantle reservoirs that are entrained and carried to the surface by mantle plumes[6], but it is unclear how individual plumes could successively sample each of these reservoirs or why the recycled oceanic crust would have variable ages. Here we use high-resolution numerical simulations to investigate the interaction between mantle plumes, subducted oceanic crust and a more primitive lower mantle reservoir. In our simulations, some subducted oceanic crust is entrained directly into mantle plumes, but a significant fraction of the crust—up to 10%—enters the more primitive reservoirs. As a result, mantle plumes entrain a variable combination of relatively young oceanic crust directly from the subducting slab, older oceanic crust that has been stirred with ancient more primitive material and background, depleted mantle. Cycling of oceanic crust through mantle reservoirs can therefore reconcile observations of different recycled oceanic crustal ages and explain the chemical complexity of hotspot lavas.

The two large low-shear-velocity provinces (LLSVPs) of the lower mantle[7–9] are hypothesized to be caused by large accumulations of intrinsically denser, more primitive material[10–14], perhaps formed by Earth's early differentiation processes[12]. This material could be swept into thermochemical piles beneath upwelling regions by Earth's subduction history[15,16]. Plumes are predicted to root from the top of these piles, entraining a small amount of more primitive material into them[11]. This conceptual framework provides an understanding for the more primitive chemical signature of ocean island basalts, but it doesn't explain the recycled oceanic crustal components (for example, high $\mu = {}^{238}\mathrm{U}/{}^{204}\mathrm{Pb}$, enriched mantle 1, enriched mantle 1; ref. 1). Previous numerical calculations have shown that the interaction between subducted oceanic crust and a dense layer of undegassed material could result in plumes entraining both components[17,18]. However, it is unclear how subducted oceanic crust would interact with the thermochemical piles that are hypothesized to cause the LLSVPs and lead to compositional heterogeneity within plumes. It is also unclear how plumes could entrain recycled oceanic crust with vastly different ages, ranging from Archaean time[4] to geologically recent[5].

We modified the two-dimensional Cartesian code CitCom[19] to include multiple thermochemical species and compositional rheology to solve the conservation equations of mass, momentum and energy in Boussinesq approximation (Supplementary Information). We employ a Rayleigh number Ra $= 1\times10^7$ for most cases. Viscosity is both depth- and temperature-dependent. A 50× viscosity increase is employed from upper mantle to lower mantle. The temperature-dependent viscosity is expressed as $\eta_T = \exp(A(0.5 - T))$, where T is non-dimensional temperature, and we use a non-dimensional activation coefficient of $A = 9.21$, leading to a 10,000× viscosity range owing to changes in temperature. Furthermore, a viscosity reduction owing to post-Perovskite (pPv) phase transition[20,21] is employed in the lowermost mantle (Supplementary Information). Supplementary Table 1 lists physical parameters for all cases used here.

The compositional field is modelled by ~7.4 million tracers using ratio tracer method[22]. To generate an appropriate initial condition, we first carry out a lower resolution (1,152 × 192 elements), two-component calculation that includes only the more primitive material and background mantle until the model comes to thermal equilibrium and large-scale thermochemical piles (composed of denser more primitive material) are developed. Then, we interpolate the temperature and composition fields to higher resolution (1,152 × 320 elements). The new mesh is refined in the very top (3 km resolution) and lowermost 1,200 km of the mantle (6 km resolution). Thereafter, we continually introduce a 6-km-thick oceanic crust near the surface of the model (Supplementary Information). All boundaries are free-slip. Temperature boundary conditions are isothermal on the top and bottom and insulating on both sides.

We define a reference case in which the oceanic crust and more primitive material have the same buoyancy number of 0.8 (about 2–3% denser than background mantle) and the viscosity of the pPv phase is reduced by 100× (in addition to the temperature-dependence of viscosity). Figure 1 shows a snapshot of the reference case well into the calculation, at 856 Myr.

Figure 1a is the temperature field with mantle velocity superimposed as arrows. Figure 1b shows the compositional field. Figure 1c shows the logarithm of viscosity; note the viscosity increase from upper to lower mantle and lenses of lowered viscosity at the base of downwellings owing to the presence of pPv. The more primitive material forms three piles in the lowermost mantle that are separated by downwellings, which carry a thin layer of oceanic crust that is ultimately incorporated into the lower thermal boundary layer and advected towards the piles.

Each pile is characterized by high temperature and undergoes vigorous internal convection. The composition of the piles is largely more primitive material (~90%) but contains oceanic crust (~2%) and background mantle (~8%; Fig. 1b). As shown in Supplementary Fig. 1, the proportion of subducted oceanic crust and background mantle within piles slightly increases with time, leading to evolving composition of the piles. Thermal plumes forming on top of the piles entrain many materials: ~2% more primitive material,

Arizona State University, School of Earth and Space Exploration, PO Box 871404, Tempe, Arizona 85287-1404, USA. *e-mail: Mingming.Li@asu.edu

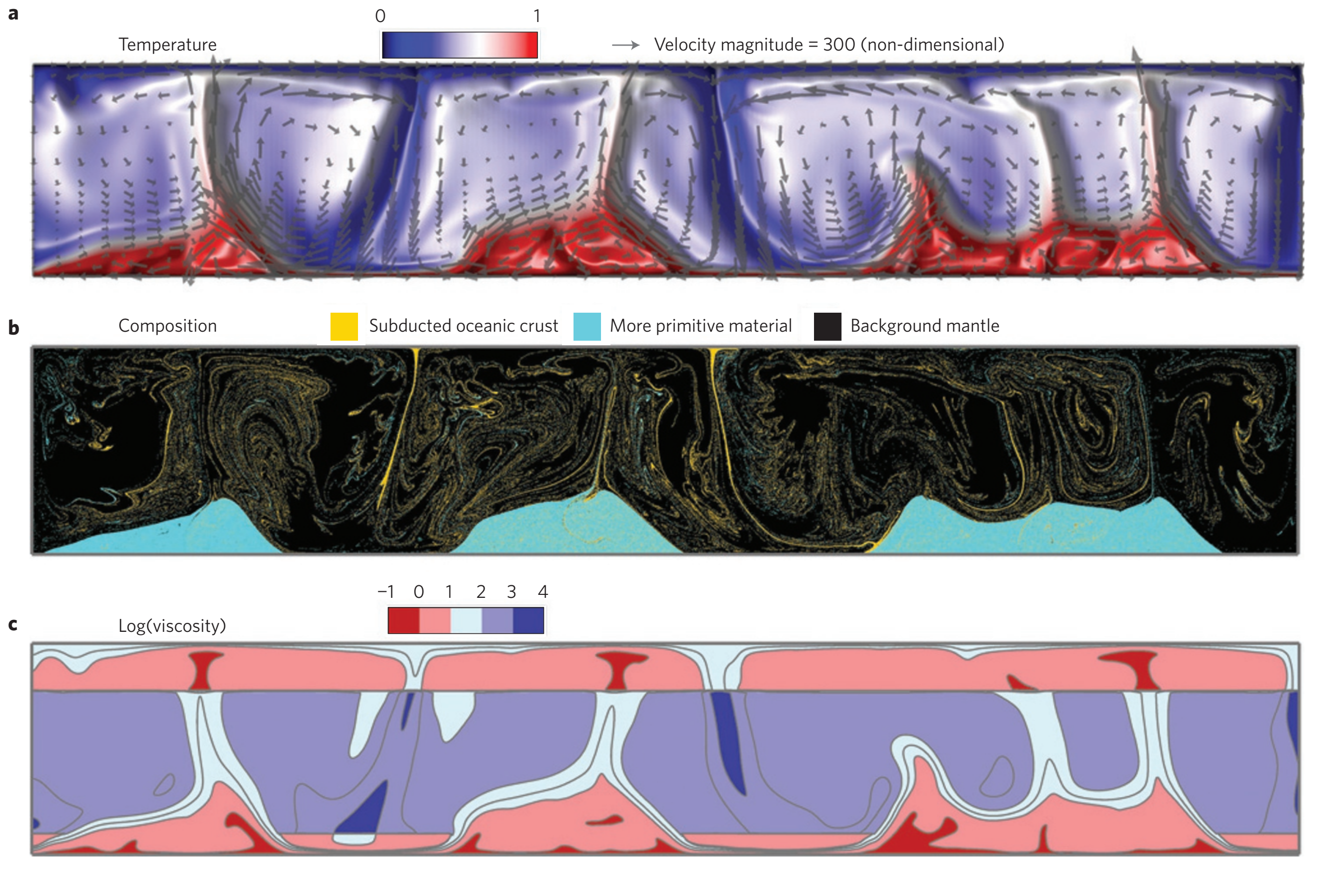

Figure 1 | Snapshot of the reference case at 856 Myr. a, Temperature field (non-dimensional) with mantle flow velocity superimposed (grey arrows). **b**, Composition field with three components: subducted oceanic crust (yellow), more primitive material (cyan) and background mantle (black). In this case, the more primitive material and subducted oceanic crust have the same density ($B = 0.8$, where B is the buoyancy number, defined in the Supplementary Information as the ratio between chemical density anomaly and density anomaly owing to thermal expansion). **c**, Logarithm of non-dimensional viscosity. Grey lines are contours with an interval of 0.5. A 100× viscosity reduction is employed for pPv, which exists near the base of downwelling regions.

~3% subducted oceanic crust (including geologically younger oceanic crust originating outside the piles and relatively older crustal material that is stirred and later entrained out with the more primitive material) and background mantle (Fig. 1b). Supplementary Fig. 2 shows the proportion of oceanic crust and more primitive material within plumes as a function of time. Outside the piles, subducted oceanic crust and material entrained from piles are stirred into the background mantle, forming a marble-cake-like texture[23].

Figure 2 shows a representative time sequence of snapshots from the reference case, illustrating how subducted oceanic crust is transported into and out of the pile and into the mantle plume. Figure 2a–c is zoomed in at the top of the central pile, in the region at the root of the mantle plume where material is exchanged between the pile and surrounding mantle. The corresponding effective buoyancy (which reflects density contributions from chemical intrinsic density and from density changes owing to thermal effects) for Fig. 2a–c is illustrated in Supplementary Fig. 3. Figure 2d,e is zoomed out for the entire central pile. Figure 2a shows a time when oceanic crust is being carried directly into the mantle plume. Furthermore, two-way material exchange is observed at the top of the pile, where pile material is being entrained into the plume and background mantle is being entrained into the pile. Figure 2b shows a later time at which oceanic crust accumulates at the base of the plume, atop the pile. After ~20 Myr, the accumulation of oceanic crust (from Fig. 2b) is flushed into the pile (Fig. 2c). A significant amount of background mantle material with positive effective buoyancy (Supplementary Fig. 3) gets trapped in this crustal package on top of the pile (Supplementary Fig. 3b) and hence gets viscously coupled and later incorporated into the pile with the crustal material (Supplementary Fig. 3c). We find this time sequence of events to be a typical process throughout all of the calculations carried out, in which the subducted oceanic crust is episodically flushed into the more primitive reservoir. Figure 2d,e shows later times at which the flushed accumulation of crust (on the scale of ~100 km) is stretched and stirred because of internal convection in the pile (Fig. 2e).

In the reference case discussed above, the oceanic crust and more primitive material have the same intrinsic density. An important question relates to how different density contrasts between the two components affect the dynamics, particularly whether they could lead to density stratification (for example, separate oceanic crust and more primitive reservoirs). In Fig. 3a–d, we show two cases in which the oceanic crust is either intrinsically less dense ($B_c = 0.6$, where B_c is the buoyancy number of the oceanic crust, Fig. 3a,b) or more dense ($B_c = 1.0$, Fig. 3c,d) than the more primitive material. We find that these two cases highly resemble the reference case and, therefore, relatively modest intrinsic density contrasts (~1%) between the oceanic crust and more primitive material do not change the fundamental dynamics. This indicates that the relevant dynamics are more controlled by viscous forces than buoyancy forces for realistically thin oceanic crust. Furthermore, we explored additional cases (Supplementary Information) in which the buoyancy number of oceanic crust ranged from $B_c = 0.0$ to $B_c = 1.2$, corresponding to ~0–4% denser than the background mantle[24]. In all cases, the relevant dynamics resembled the reference

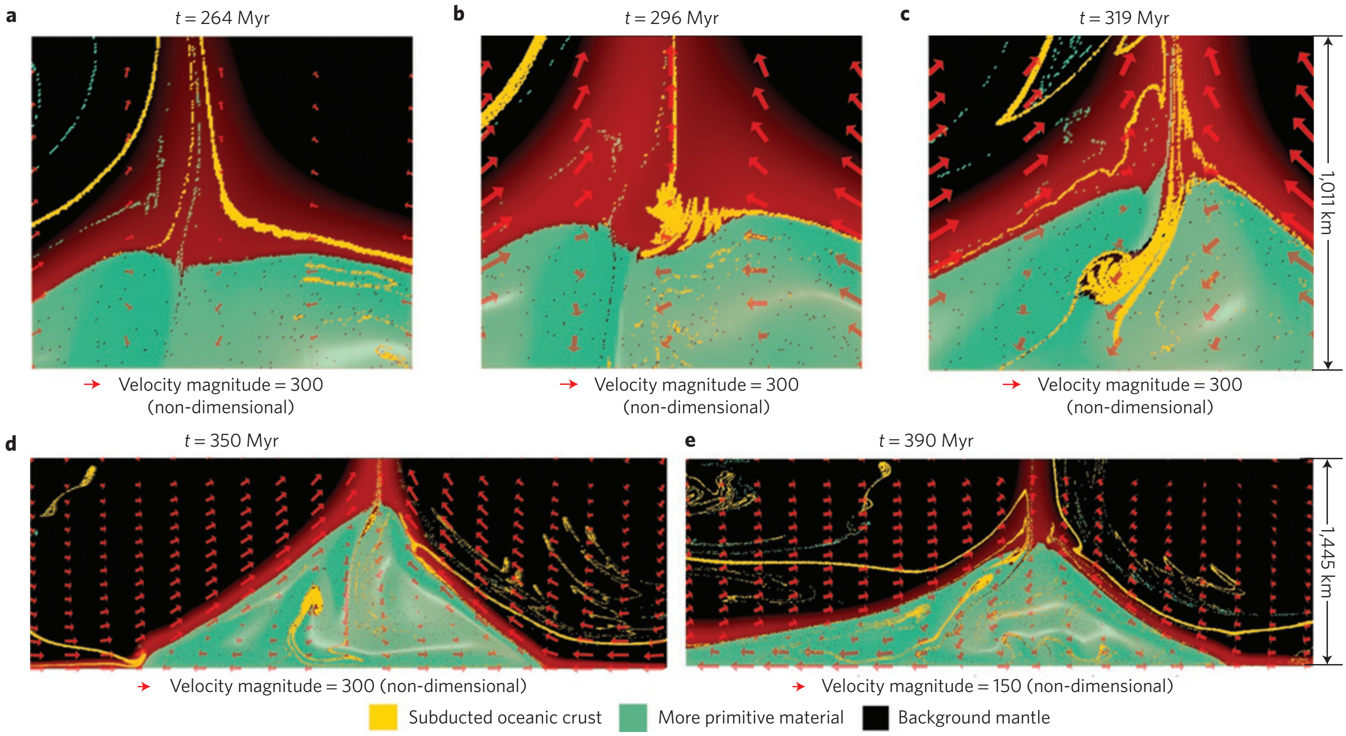

Figure 2 | Sequence of snapshots for the reference case, showing numerous pathways for subducted oceanic crust. All panels show the compositional field as the background (yellow for subducted oceanic crust, cyan for more primitive material, and black for background mantle). Superimposed on the compositional field is a partially transparent temperature field (red) shown only for non-dimensional temperatures greater than 0.5, effectively outlining the highest temperature regions: pile and thermal boundary layer and plume atop the pile. Within the pile, this temperature field is plotted as a rubber sheet, extending out of the page for higher temperatures and into the page for lower temperatures, producing a three-dimensional shading effect. Mantle flow velocity is represented by red arrows. **a–c**, Zoomed-in panels showing regions around the top of the central pile (Fig. 1). **d–e**, Zoomed-out panels showing the entire central pile. The composition field for **a–c** is also shown in Supplementary Fig. 4. Time, *t*.

case, characterized by numerous, alternative pathways of oceanic crust that is either directly entrained into upwelling plumes, episodically flushed into the more primitive reservoir, or stirred into the background mantle. Nevertheless, we did find that the fraction of subducted oceanic crust within the piles increases with the intrinsic density of oceanic crust, as shown in Fig. 4.

Figure 4 shows the percentage of total oceanic crust that resides within piles as a function of time. It is important to note that relative differences are more meaningful than absolute values because the magnitude of entrainment is somewhat dependent on mesh resolution (as is typical in numerical models), even for these high-resolution calculations. In all cases, the percentage is zero near the beginning because it takes a finite amount of time for the crust to descend into the lower mantle before being incorporated into piles. After about 350 Myr, the reference case (solid black line) is characterized by about 7–10% of oceanic crust being incorporated into the piles.

Figure 4 also shows how the viscosity of the pPv phase significantly influences the amount of oceanic crust that is incorporated into piles. The reference case employed a 100× viscosity reduction in the pPv phase that allowed oceanic crust to go deeper into the lower thermal boundary layer[25,26], where it is dragged closer to the pile surface by mantle flow and more easily incorporated into the pile. As we lessen the viscosity reduction of the pPv phase, oceanic crust doesn't penetrate the lower thermal boundary layer as deeply and, therefore, the amount of oceanic crust being incorporated into the piles is reduced.

Here, we varied the buoyancy number of oceanic crust and the intrinsic viscosity reduction associated with the pPv phase, both being parameters expected to play important, first-order roles in the underlying dynamics associated with this study. We found that although these parameters controlled the amount of oceanic crust that is incorporated into piles, the fundamental dynamical process remained unchanged. We also investigated parameters such as the Rayleigh number, the temperature-dependence of viscosity, the amount of internal heating and the buoyancy number of more primitive material, which lead to only second-order effects as expected (Supplementary Figs 5–14).

Here we show how subducted oceanic crust interacts with long-lived, originally more primitive compositional reservoirs (which are hypothesized to cause the LLSVPs). We show that oceanic crust first enters the lowermost thermal boundary layer at the core–mantle boundary in downwelling regions and is then transported laterally towards and then up along the surface of the piles. At the top of the piles where plumes are rooted, the oceanic crust is either entrained into plumes (along with material from the pile) or flushed into the pile. This process seems to be dominated by viscous forces and is relatively insensitive to density contrasts between the oceanic crust and more primitive material.

In the piles, oceanic crust is continually stirred within the more primitive material, leading to multiscale compositional heterogeneity in space and time. This could possibly contribute to seismic heterogeneity and/or discontinuities within LLSVPs as is observed by seismic studies[27,28]. In particular, future seismological studies should focus on the tops of LLSVPs, where the oceanic crust may be detected. More notably, this heterogeneity would be reflected in hotspot basalt chemistry because mantle plumes would entrain a time-variable combination of different compositions, including relatively young oceanic crust, older oceanic crust that was flushed into the pile at an earlier time, ancient, more primitive reservoir

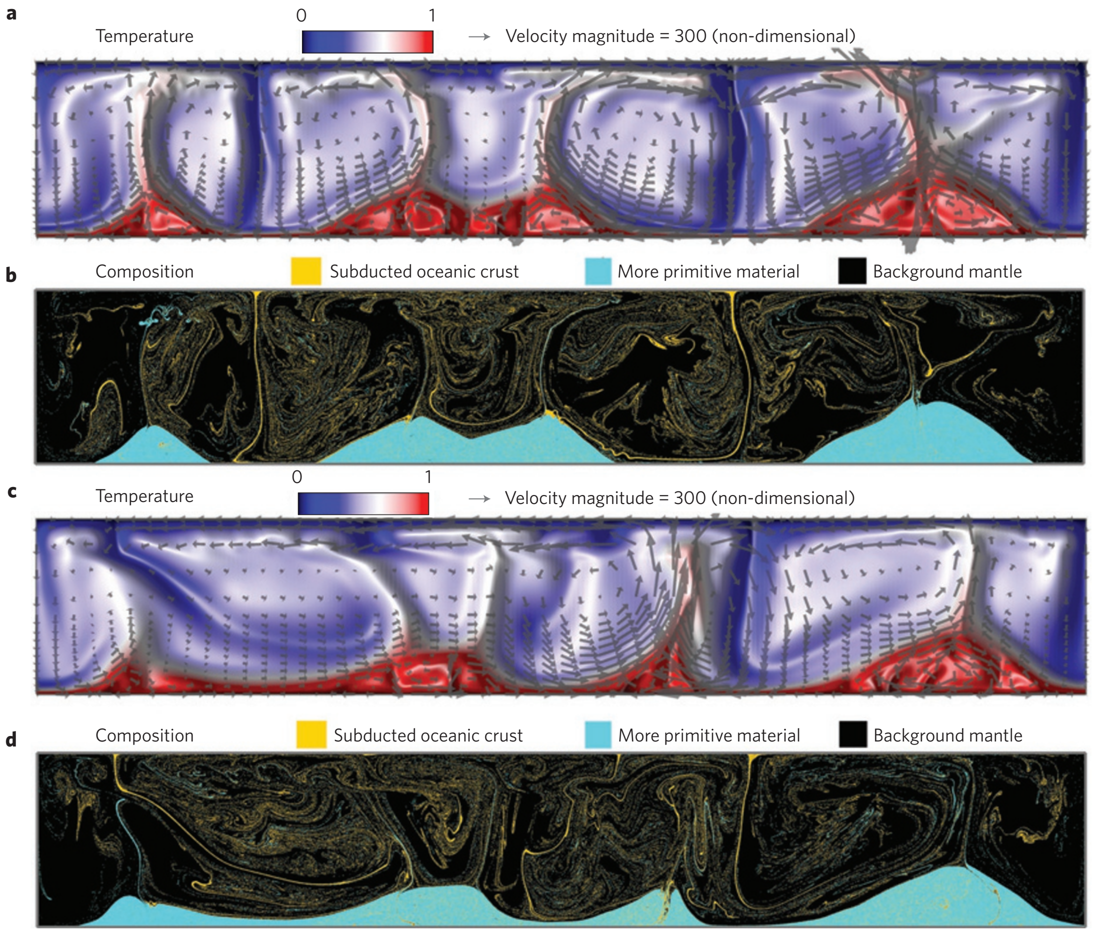

Figure 3 | Effects of intrinsic density contrast between more primitive material and subducted oceanic crust. a–b, Snapshot (880 Myr) of the case in which subducted oceanic crust is less dense ($B = 0.6$) than the more primitive reservoir ($B = 0.8$). **c–d**, Snapshot (840 Myr) of the case in which subducted oceanic crust is more dense ($B = 1$) than the more primitive reservoir ($B = 0.8$). **a**,**c**, Temperature field with mantle flow velocity superimposed (grey arrows). **b**,**d**, Composition field.

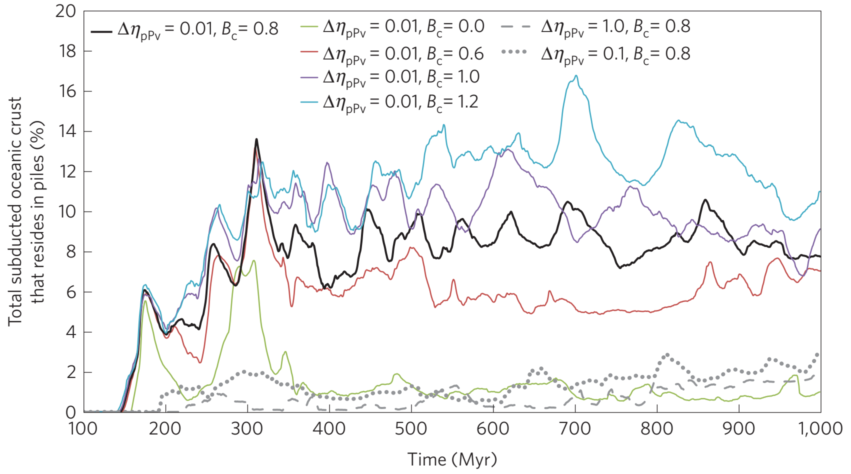

Figure 4 | Percentage of total oceanic crust that resides in piles as a function of time. $\Delta\eta_{pPv}$, viscosity reduction due to the pPv phase. Bc, buoyancy number of the oceanic crust.

material and depleted background mantle. Furthermore, plumes sampling geographically different parts of the LLSVPs could have different compositions[29]. These factors provide an explanation for the spatial and temporal variability of trace element chemistry in hotspot basalts[1,29,30] and provide an understanding of why signatures of oceanic crust in hotspot basalts can range from Archaean age[4] to geologically recent[5].

Received 7 November 2013; accepted 18 February 2014; published online 30 March 2014

References

1. Hofmann, A. W. Mantle geochemistry: The message from oceanic volcanism. *Nature* **385,** 219–229 (1997).
2. Jackson, M. G. *et al.* Evidence for the survival of the oldest terrestrial mantle reservoir. *Nature* **466,** 853–856 (2010).
3. Mukhopadhyay, S. Early differentiation and volatile accretion recorded in deep-mantle neon and xenon. *Nature* **486,** 101–104 (2012).
4. Cabral, R. A. *et al.* Anomalous sulphur isotopes in plume lavas reveal deep mantle storage of Archaean crust. *Nature* **496,** 490–493 (2013).
5. Sobolev, A. V., Hofmann, A. W., Jochum, K. P., Kuzmin, D. V. & Stoll, B. A young source for the Hawaiian plume. *Nature* **476,** 434–437 (2011).
6. Tackley, P. J. Mantle convection and plate tectonics: Toward an integrated physical and chemical theory. *Science* **288,** 2002–2007 (2000).
7. Dziewonski, A. M., Lekic, V. & Romanowicz, B. A. Mantle anchor structure: An argument for bottom up tectonics. *Earth Planet. Sci. Lett.* **299,** 69–79 (2010).
8. He, Y. & Wen, L. Geographic boundary of the 'Pacific Anomaly' and its geometry and transitional structure in the north. *J. Geophys. Res.* **117,** B09308 (2012).
9. Garnero, E. J. & McNamara, A. K. Structure and dynamics of Earth's lower mantle. *Science* **320,** 626–628 (2008).
10. Tackley, P. in *The Core-Mantle Boundary Region* (ed. Gurnis, M.) 231–253 (AGU Geophysical Monograph, 1998).
11. Deschamps, F., Kaminski, E. & Tackley, P. J. A deep mantle origin for the primitive signature of ocean island basalt. *Nature Geosci.* **4,** 879–882 (2011).
12. Labrosse, S., Hernlund, J. W. & Coltice, N. A crystallizing dense magma ocean at the base of the Earth's mantle. *Nature* **450,** 866–869 (2007).
13. Deschamps, F., Cobden, L. & Tackley, P. J. The primitive nature of large low shear-wave velocity provinces. *Earth Planet. Sci. Lett.* **349–350,** 198–208 (2012).
14. Torsvik, T. H., Burke, K., Steinberger, B., Webb, S. J. & Ashwal, L. D. Diamonds sampled by plumes from the core–mantle boundary. *Nature* **466,** 352–355 (2010).
15. Bull, A. L., McNamara, A. K. & Ritsema, J. Synthetic tomography of plume clusters and thermochemical piles. *Earth Planet. Sci. Lett.* **278,** 152–162 (2009).
16. McNamara, A. K. & Zhong, S. Thermochemical structures beneath Africa and the Pacific Ocean. *Nature* **437,** 1136–1139 (2005).
17. Samuel, H. & Farnetani, C. G. Thermochemical convection and helium concentrations in mantle plumes. *Earth Planet. Sci. Lett.* **207,** 39–56 (2003).
18. Tackley, P. J. Living dead slabs in 3-D: The dynamics of compositionally-stratified slabs entering a 'slab graveyard' above the core–mantle boundary. *Phys. Earth Planet. Inter.* **188,** 150–162 (2011).
19. Moresi, L. & Gurnis, M. Constraints on the lateral strength of slabs from three-dimensional dynamic flow models. *Earth Planet. Sci. Lett.* **138,** 15–28 (1996).
20. Ammann, M. W., Brodholt, J. P., Wookey, J. & Dobson, D. P. First-principles constraints on diffusion in lower-mantle minerals and a weak D' layer. *Nature* **465,** 462–465 (2010).
21. Hunt, S. A. *et al.* Weakening of calcium iridate during its transformation from perovskite to post-perovskite. *Nature Geosci.* **2,** 794–797 (2009).
22. Tackley, P. J. & King, S. D. Testing the tracer ratio method for modeling active compositional fields in mantle convection simulations. *Geochem. Geophys. Geosyst.* **4,** 8302 (2003).
23. Allegre, C. J. & Turcotte, D. L. Implications of a two-component marble-cake mantle. *Nature* **323,** 123–127 (1986).
24. Hirose, K., Takafuji, N., Sata, N. & Ohishi, Y. Phase transition and density of subducted MORB crust in the lower mantle. *Earth Planet. Sci. Lett.* **237,** 239–251 (2005).
25. Li, M. M. & McNamara, A. K. The difficulty for subducted oceanic crust to accumulate at the Earth's core–mantle boundary. *J. Geophys. Res.* **118,** 1807–1816 (2013).
26. Nakagawa, T. & Tackley, P. J. Effects of low-viscosity post-perovskite on thermo-chemical mantle convection in a 3-D spherical shell. *Geophys. Res. Lett.* **38,** L04309 (2011).
27. Lay, T., Hernlund, J., Garnero, E. J. & Thorne, M. S. A post-perovskite lens and D' heat flux beneath the central pacific. *Science* **314,** 1272–1276 (2006).
28. Ohta, K., Hirose, K., Lay, T., Sata, N. & Ohishi, Y. Phase transitions in pyrolite and MORB at lowermost mantle conditions: Implications for a MORB-rich pile above the core–mantle boundary. *Earth Planet. Sci. Lett.* **267,** 107–117 (2008).
29. Weis, D., Garcia, M. O., Rhodes, J. M., Jellinek, M. & Scoates, J. S. Role of the deep mantle in generating the compositional asymmetry of the Hawaiian mantle plume. *Nature Geosci.* **4,** 831–838 (2011).
30. Farnetani, C. G., Legras, B. & Tackley, P. J. Mixing and deformations in mantle plumes. *Earth Planet. Sci. Lett.* **196,** 1–15 (2002).

Acknowledgements

We thank F. Deschamps and C. G. Farnetani for their reviews. This work is supported by NSF grant EAR-1045788 and EAR-1161038.

Author contributions

All authors contributed to conceiving the idea and writing the paper. M.L. carried out the numerical calculation. A.K.M. supervised the project.

Additional information

Supplementary information is available in the online version of the paper. Reprints and permissions information is available online at www.nature.com/reprints. Correspondence and requests for materials should be addressed to M.L.

Competing financial interests

The authors declare no competing financial interests.